www.springer.com/41230
https://doi.org/10.1007/s41230-022-1117-z

Effect of Gd content on hot-tearing susceptibility of Mg-6Zn-*x*Gd casting alloys

He Qin[1], *Guang-yu Yang[1], Xun-wei Zheng[2], Shi-feng Luo[1], Tong Bai[1], and Wan-qi Jie[1]

1. State Key Laboratory of Solidification Processing, Northwestern Polytechnical University, Xi'an 710072, China

2. Dongfeng Nissan Aeolus Xiangyang Automobile Co., Ltd., Xiangyang 441100, Hubei, China

Abstract: The hot-tearing susceptibility (HTS) of Mg-6Zn-*x*Gd (*x*=0.5, 1, 2, 3, 4, 6) alloys was evaluated using a constrained rod casting (CRC) method. The results show that the HTS curve follows a typical "Λ" shape with the increase of Gd content. The Mg-6Zn-2Gd alloy has the highest while Mg-6Zn-6Gd alloy has the lowest HTS value. The hot-tearing behavior characteristics of Mg-6Zn-*x*Gd alloys were further studied through a multifunctional hot-tearing test device. According to the dendrite contact point inferred from the stress curve, the Clyne-Davies criterion was modified and found to be accurate in predicting the HTS of Mg-6Zn-*x*Gd alloys. Microstructure observation reveals that the grain size and the volume of eutectic liquid are the two key factors affecting HTS of Mg-6Zn-*x*Gd alloys. The large grain with columnar structure can easily promote initiation and propagation of hot-tearing due to the poor feeding and coordinating deformation capability, which have a harmful effect on HTS. A higher volume fraction of eutectic phase can refill the cracking and provide continuous feeding channels by dendrite bridge and thicker liquid film, thus increase the hot-tearing resistance.

Keywords: Mg-Zn-Gd alloy; hot-tearing susceptibility; modified Clyne-Davies model; microstructure

CLC numbers: TG146.22 **Document code:** A **Article ID:** 1672-6421(2022)02-131-09

1 Introduction

As the lightest available structural material, magnesium (Mg) alloys have recently attracted significant interest due to their excellent specific properties that make them potentially suitable candidates for replacing heavier materials in aerospace and automotive industries [1-3]. In particular, Mg-Zn based casting alloys are showing a promising engineering application prospect for their good balance between costs and high strength [4, 5]. However, as a major casting defect, hot tearing often occurs during the casting of Mg-Zn based alloys because of large crystallization temperature range, coarse grains and grain boundary defects, which significantly limits their wide applications in engineering fields [6, 7].

In the last decades, many studies have been conducted to investigate the hot-tearing susceptibility (HTS) of Mg-Zn based alloys. Clyne et al. [8] carried out the preliminary investigations on the HTS of binary Mg-Zn alloy and concluded that the largest HTS could be observed with 2% Zn (in weight, unless specified). Zhou et al. [9] found that the HTS of binary Mg-Zn alloy decreased with the increase of the initial mold temperature. Recently, researchers have found that multiple rare earth (RE) elements, such as Gd, Y, and Nd, not only improve the high temperature performance, but also reduce the HTS of Mg-Zn based casting alloys. Wang et al. [10] investigated the effect of Y addition on the HTS of Mg-Zn alloys, and found that the HTS decreased with Y content increasing from 0.9% to 2%, which was attributed to the effective crack healing by eutectic liquid at the final stage of solidification. Gunde et al. [11] also confirmed Y addition had a positive effect on preventing the hot tearing of Mg-3Zn-0.5Zr alloys due to the increased solidus temperature, shortened terminal solidification path and reduced terminal freezing range. Comparing with Y element, Gd addition has been used more often since Gd can form some high thermal stability phases with Mg and Zn besides the high solid solution of Gd in the Mg matrix [12, 13]. Mg-Zn-Gd alloys exhibit good mechanical properties at both room and elevated temperatures [14, 15]. Srinivasan [16] and Luo et al. [17] studied the HTS of binary Mg-Gd alloys with different Gd contents by a constrained rod casting (CRC) mold, they found that the HTS versus Gd content followed a typical "Λ" curve, i.e., increased firstly and then decreased. However, there are very

***Guang-yu Yang**

Male, born in 1967, Ph.D., Professor. His research interests mainly focus on the development of high strength Mg and Al cast alloys, and liquid metal forming technology. To date, he has published more than 40 technical papers.

E-mail: ygy@nwpu.edu.cn

Received: 2021-07-09; Accepted: 2021-11-23

limited information available in the literature about the effect of Gd addition on hot tearing of the Mg-Zn alloy. Therefore, it is very necessary to evaluate and study the hot tearing of Mg-Zn-Gd casting alloy.

In this work, the HTS of ternary Mg-6Zn-*x*Gd (*x*=0.5, 1, 2, 3, 4, 6) casting alloys was investigated using a CRC mold and a multifunctional hot-tearing test device with a load cell and data acquisition system, and the important factors affecting HTS of Mg-6Zn-*x*Gd alloys were discussed.

2 Experimental procedure

Pure Mg (99.9%), pure Zn (99.95%), and Mg-28Gd master alloy were used to prepare Mg-6Zn-*x*Gd (*x*=0.5, 1, 2, 3, 4, 6) alloys in an electrical-resistance furnace under a productive gas of CO_2+0.1% SF_6. The preheated pure Zn was added to pure magnesium melt at 700 °C, and Mg-28Gd master alloy was added at 760 °C. Then, the melt was held at 760 °C for 20 min followed by cooling to 740 °C for C_2Cl_6 refining. Finally, the melt was poured into the preheated CRC steel mold (200 °C) or sand casting mold (room temperature) with a multifunctional testing device at 720 °C. The chemical compositions of Mg-6Zn-*x*Gd alloys are listed in Table 1, which are determined through the inductively coupled plasma atomic emission spectrum (ICP-AES) apparatus.

Figure 1 shows the schematic diagram of the CRC steel mold. It allows four rods of 10 mm in diameter with different lengths of 51, 89, 127 and 165 mm and a constant spacing of 38 mm is kept between the two adjacent rods. The end of each rod is attached with a ball of 20 mm in diameter, which acts as an anchor to restrain the rod from free contraction during casting.

According to previous research results, HTS of the experimental alloys can be evaluated by the following Eq. (1) [18]:

$$HTS=\Sigma(f_{tear}\times f_{length}\times f_{location}) \quad (1)$$

where f_{tear} is the tear width factor with 1 for short hair line (a hairline crack), 2 for full hair line, 3 for half broken and 4 for totally broken; f_{length} is the tear length factor, where the 4, 8, 16, 32 are the longest rod, second longest rod, third longest rod, the shortest rod, respectively, as shown in Fig. 2(a); $f_{location}$ is the tear location factor, where 1, 2, 3 are the tearing at the sprue end, at the ball end, in the middle of the rod, respectively, as shown in Fig. 2(b). Three times were repeated at each condition, and the average value was taken as the measuring result.

The multifunctional testing device consists of a sand mold system and a data acquisition system, as shown in Fig. 3(a). The data acquisition system can record the change of contraction force by a load cell during alloy solidification. The casting mold made by sand mixed with 2% resin and 0.4% curing agent. The solidification stress curves of the testing alloys were obtained through the load sensor. The size and geometry of the "I-shaped" casting specimen are shown in Fig. 3(b), which is designed to capture the hot tearing in the variable section. A K-type thermocouple was attached on the variable section to record temperature variation at the place where hot tearing

Table 1: Chemical compositions of tested alloys (wt.%)

Alloy	Zn	Gd	Mg
Mg-6Zn-0.5Gd	5.84	0.42	Bal.
Mg-6Zn-1Gd	6.21	1.14	Bal.
Mg-6Zn-2Gd	5.96	2.21	Bal.
Mg-6Zn-3Gd	6.04	3.18	Bal.
Mg-6Zn-4Gd	6.11	3.98	Bal.
Mg-6Zn-6Gd	5.89	6.07	Bal.

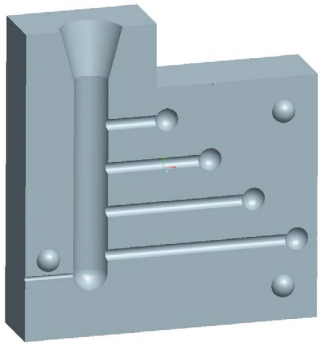

Fig. 1: Schematic diagram of CRC steel mold

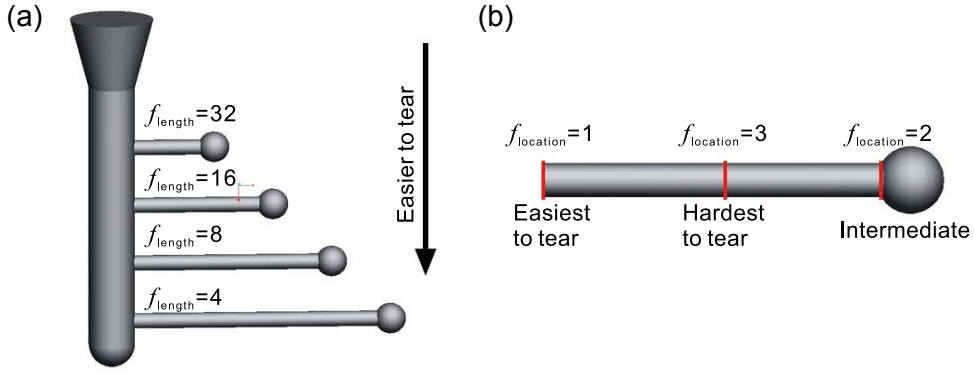

Fig. 2: Schematic of hot tearing factors at different positions in CRC method: (a) rod length factor, (b) tear location factor

occurs. The specimen was fixed by two nail at each end of the rod. The sprue was connected on the thick side of the rod with the diameter of 35 mm. The diameter of thin side of the rod was 20 mm.

Transversal section [as shown in Fig. 3(b)] of the "I-shaped" casting rod near the tearing section was selected for the grain size measurement and microstructure observation. The polished samples were chemically etched in a solution of 8 g picric acid, 5 mL acetic acid, 10 mL distilled water, and 100 mL ethanol, and then were examined by Olympus PM-G3 type optical microscopy (OM), and JEOL JSM-5800 scanning electron microscopy (SEM) equipped with an electron dispersive spectrometer (EDS). The grain sizes were measured five times by linear intercept method, and the average value was taken as the measuring result.

3 Results and discussion

3.1 HTS of Mg-Zn-*x*Gd casting alloys

Figure 4 shows the typical CRC casting rods and the magnified pictures of sprue and ball ends for Mg-6Zn-2Gd alloy, where the hot tears are marked in red rectangles. The tears near the sprue in Fig. 4(b) shows that full hair line and short hair line are observed in the first and second sprues, respectively. In Fig. 4(a), the half broken is observed in the third rod. In Fig. 4(c), the short hair line, full hair line and totally broken are observed in the second, third and fourth ball, respectively.

Based on Eq. (1), the HTS of Mg-6Zn-*x*Gd alloys can be calculated quantitatively. The relationship between the calculated HTS value and Gd content is shown in Fig. 5. A typical "Λ" shaped curve is observed: HTS increases firstly with the increase of Gd content until Gd content reaching 2%, and then decreases with further increasing Gd content to 6%. Mg-6Zn-2Gd alloy and Mg-6Zn-6Gd alloy have the highest and the lowest HTS values, respectively.

3.2 Solidification characteristics of Mg-Zn-*x*Gd casting alloys

To further understand the hot-tearing behavior characteristics of Mg-6Zn-*x*Gd alloys, a multifunctional hot-tearing test device was used to obtain the typical solidification characteristic curves (including the temperature curves and load curves) of the experimental alloys. As shown in Fig. 6, in the load curves, the suddenly rising contraction load represents the dendrite contacting each other and a dropping contraction load represents the propagation of hot tearing [7, 19]. In addition, the position where contraction load curve transforms from linear increment to non-linear increment can be considered as the onset of hot tearing initiation [20]. Furthermore, the solid fraction curves in Fig. 6 was determined by Newton's baseline criterion [6, 21-23].

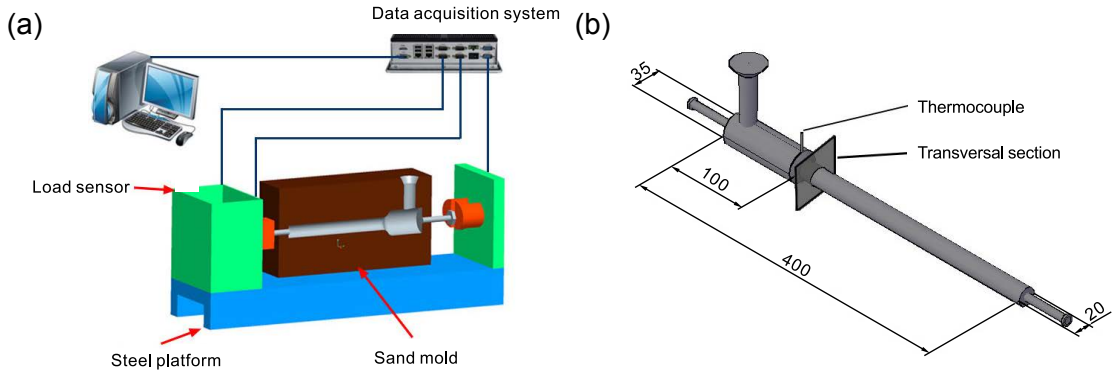

Fig. 3: Schematics of multifunctional device (a), and "I-shaped" casting specimen (unit: mm) (b)

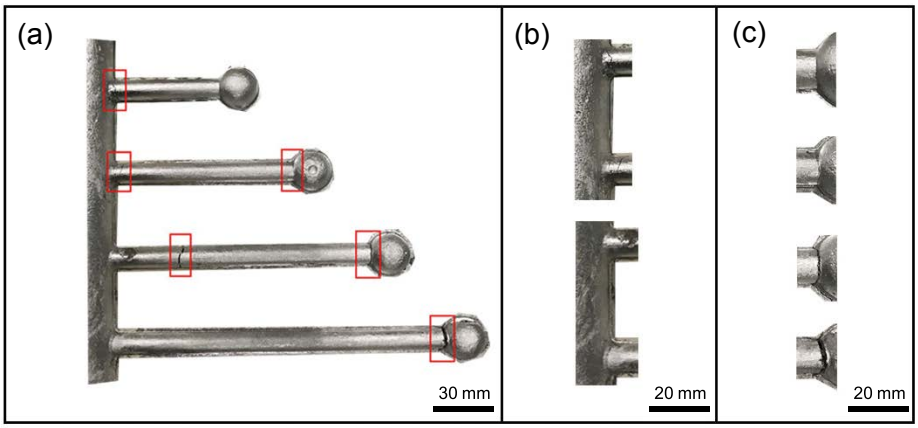

Fig. 4: Macro morphology of hot tear in Mg-6Zn-2Gd casting alloy (a), close-up view of tears near the spure (b), and close-up view of tears at the ball ends of rods (c)

Figure 6(a) shows the solidification characteristic curves of Mg-6Zn-0.5Gd alloy. It can be seen that load increases sharply at the temperature of 562.5 °C with the solid fraction of 0.735 (1 represents complete solidification). As the temperature decreases to 526 °C with the solid fraction of 0.829, the increase of load becomes very slow. Owing to the enough remaining eutectic liquid, the first onset of hot tearing initiation can be filled. The increase of load becomes slow again at 491 °C when the solid fraction is 0.880, indicating the second onset of hot tearing initiation. Due to the less eutectic liquid at this time, the second hot tearing could not be filled in time, which causes the crack initiation. The initiated crack gradually connected together by propagation. Then, the casting bar is gradually torn up partially. When the content of Gd increases to 1%, the dendrites contact each other at 573 °C, which corresponds to a solid fraction of 0.669, as shown in Fig. 6(b). Hot tearing initiates at 564 °C and 519 °C, and the corresponding solid fraction is 0.715 and 0.833, respectively. After the formation of hot tearing, the load line turns into smooth and keeps basically unchanged till the end of solidification. Mg-6Zn-2Gd alloy bar totally breaks up and the load line does not rise up,

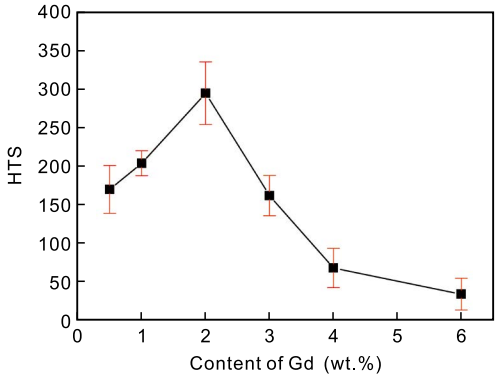

Fig. 5: HTS of Mg-6Zn-*x*Gd tested alloys as a function of Gd content

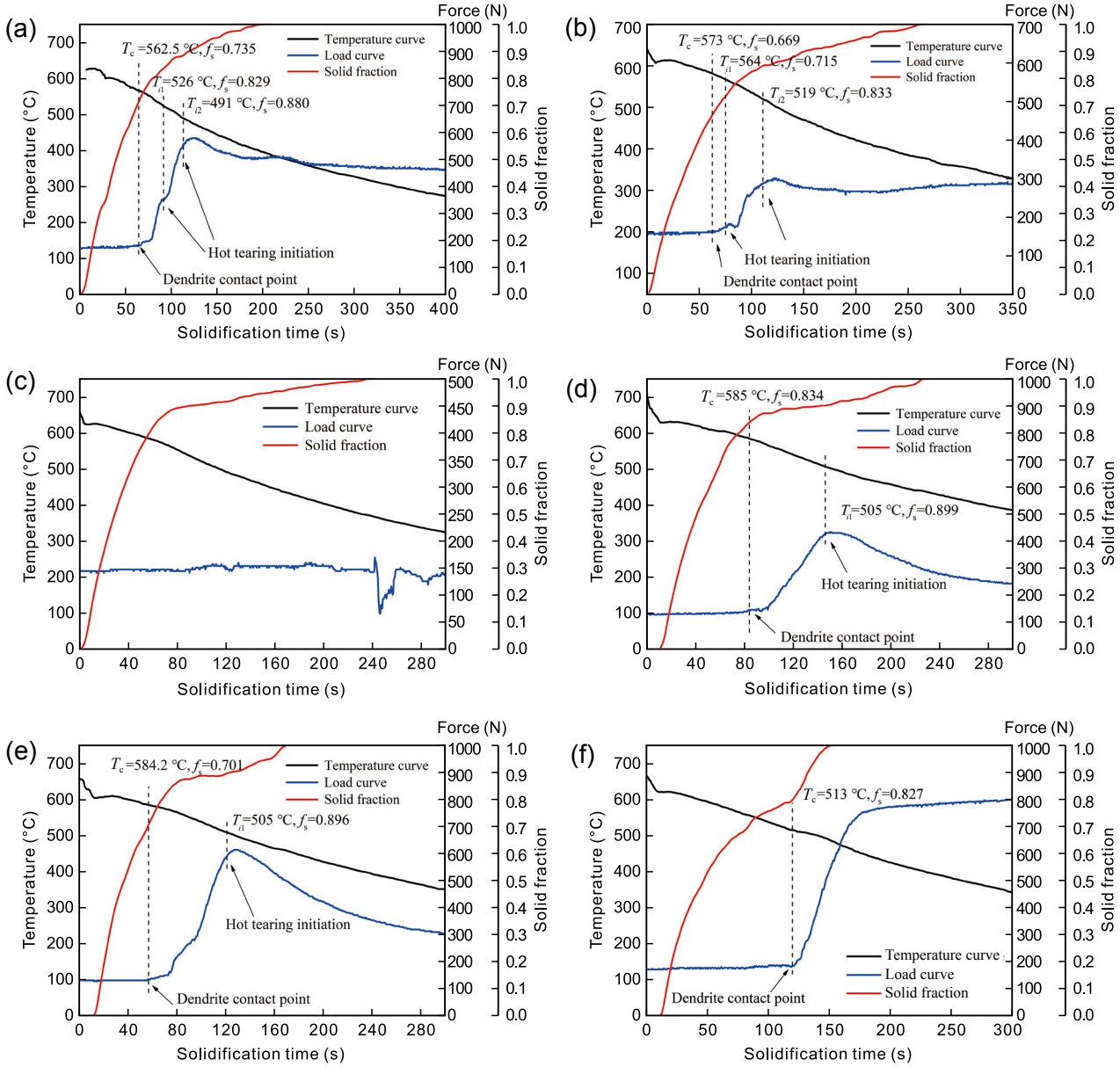

Fig. 6: Solidification characteristic curves of Mg-6Zn-*x*Gd alloys: (a) *x*=0.5, (b) *x*=1, (c) *x*=2, (d) *x*=3; (e) *x*=4, and (f) *x*=6

as shown in Fig. 6(c). For Mg-6Zn-3Gd alloy [Fig. 6(d)], the hot tearing initiates at 585 °C where the dendrites are contacted and the solid fraction is 0.834. At 505 °C and the solid fraction of 0.899, the hot tearing forms and propagates gradually. Finally, the casting bar is torn up. Figure 6(e) is the solidification characteristic curves of Mg-6Zn-4Gd alloy, where the dendrites contact at 584.2 °C and the solid fraction is 0.701. The hot tearing occurs at 505 °C, corresponding to a solid fraction of 0.896. When the content of Gd reaches 6%, the dendrites contact at 513 °C and the solid fraction is 0.827, as shown in Fig. 6(f), and no hot tearing occurs. In addition, the obtained data of the fracture stress can also reflect the hot-tearing resistance. The fracture stresses of Mg-6Zn-0.5Gd, Mg-6Zn-4Gd, Mg-6Zn-6Gd alloys reach 500 N and other alloys are less than 500 N, as shown in Fig. 6, indicating that the Mg-6Zn-*x*Gd (*x*=0.5, 4, 6) alloys have higher hot tearing resistance.

Clyne and Davies et al. [8, 24] have proposed a hot tearing criterion called cracking susceptibility coefficient (CSC), which can be expressed as:

$$\mathrm{CSC}=\frac{t_{\mathrm{V}}}{t_{\mathrm{R}}}=\frac{t_{0.99}-t_{0.9}}{t_{0.9}-t_{0.4}} \tag{2}$$

where t_{V} is the time period of the stress release process in vulnerable region, t_{R} is the time period of the stress release process in stress relaxation region, and $t_{0.4}$, $t_{0.9}$, $t_{0.99}$ are the time when solid fraction is up to 0.4, 0.9, 0.99, respectively. When the liquid fraction is less than 0.4, dendritic grain is formed and dispersed. With the solidification process continuing, isolated dendritic grains contact each other and the remaining liquid can feed the tear caused by interdendritic solidification shrinkage. This stage is known as stress relaxation and can be defined as t_{R}, during which the solid fraction is between 0.4 and 0.9. In the later stage of solidification, solid fraction is between 0.9 and 0.99 and the liquid is too low to feed the hot tearing caused by solidification shrinkage. This stage is defined as vulnerable region, and the corresponding solidification time is defined as t_{V}.

It should be noted that the CSC criterion assumes that the dendrites contact each other when the solid fraction is 0.4 (f_{S}=0.4). However, the dendrite contact point varies with the composition of the alloy. Researchers have developed some new methods to detect the real dendrite contact point, such as double thermocouple method, which can accurately determine the dendrite contact time [23]. It suggests that the heat transfer rate increases significantly with the proceeding of solidification when the dendrites come into contact each other, because solid has higher thermal conductivity. And this change can be measured easily. In addition, the dendrite coherency can lead to the stress curve suddenly change. Thus, in this study, the time when stress curve rises can be regarded as dendrite coherency point (t_{DCP}), and the corresponding temperature is called the temperature of dendrite coherency point (T_{DCP}). Based on the solidification characteristic curves of Mg-6Zn-*x*Gd alloys, the hot tearing characteristic parameters of Mg-6Zn-*x*Gd casting alloys are summarized in Table 2, where f_{DCP} is solid fraction when dendrites contact with each other and t_x is the time when the solid fraction is "*x*". The modified CSC criterion is thus defined as hot-tearing susceptibility coefficient (HSC):

$$\mathrm{HSC}=\frac{t_{0.99}-t_{0.9}}{t_{0.9}-t_{\mathrm{DCP}}} \tag{3}$$

Combined the Eq. (3) with the experimental results in Table 2, the calculated results of HSC values for Mg-6Zn-*x*Gd (*x*=0.5, 1, 2, 3, 4, 6) casting alloys are 1.115, 1.224, 2.322, 0.750, 0.599 and 0.512, respectively. Among them, the bar of Mg-6Zn-2Gd alloy is totally broken and the load change isn't detected at all, therefore the solid fraction of dendrite coherency point for Mg-6Zn-2Gd alloy is supposed to be 0.7, the average of this experiment. The HTS curves of the experimental alloys are also plotted in Fig. 7(a). It can be seen that the HTS and HSC curves present a similar typical "Λ" shape and all curves increase firstly with increasing Gd content, reaching the maximum at 2% Gd, and then decrease. Linear regression analysis between HSC and HTS is shown in Fig. 7(b), and the mathematical relationship can be described as:

$$\mathrm{HSC}=0.066+0.0066\times\mathrm{HTS} \tag{4}$$

A high degree of correlation is found (R^2=0.82), which further indicates that the modified HSC criterion is suitable for predicting hot-tearing susceptibility of Mg-6Zn-*x*Gd ternary alloys.

3.3 Microstructural observation

Grain size and morphology are important parameters influencing the HTS, which will affect the liquid metal feeding process [16, 17]. Figure 8 shows OM images of Mg-6Zn-*x*Gd casting alloys taken from the cross section of "I-shaped" rod. From Figs. 8(a) to (f), it can be found with the increase of Gd content, the grain size increases firstly and reaches the maximum at 2% Gd, and then decreases and reaches the minimum at 6% Gd. The variation of grain size (*d*) with the Gd content is shown in Fig. 9(a). As shown in Fig. 8(a), fine

Table 2: Hot-tearing characteristic parameters of Mg-6Zn-*x*Gd casting alloys

Parameters	Mg-6Zn-0.5Gd	Mg-6Zn-1Gd	Mg-6Zn-2Gd	Mg-6Zn-3Gd	Mg-6Zn-4Gd	Mg-6Zn-6Gd
t_{DCP} (s)	89.2	73.5	46.5	93.5	56.5	112.5
f_{DCP}	0.735	0.673	0.700	0.834	0.701	0.827
$t_{0.9}$ (s)	121.0	157.0	102.5	167.5	127.5	130.7
$t_{0.99}$ (s)	189.0	259.2	232.5	223.0	167.2	140.0

columnar grains in the outer area and equiaxed grains in the bottom right area are observed. When Gd content reaches 1%–2%, the coarse columnar grains are observed, as shown in Figs. 8(b) and (c). The grains present the similar structure with Fig. 8(a) when Gd content varies from 3%–4%. Further increasing Gd content up to 6%, entirely equiaxed grains are found, as shown in Fig. 8(f). There is a very interesting phenomenon that the crystal morphology changes from mixed grains to columnar grains, mixed grains, and equiaxed grains with increasing Gd content. Zn atoms can play an important role in grain refinement at low Gd content [25]. With the increasing content of Gd, Gd atom preferentially reacts with Zn atom to form Zn-Gd phase, due to the electronegativity difference between Gd and Zn being greater than that between Gd and Mg. In addition, the residual Zn almost dissolves in the α-Mg matrix. When further increasing Gd content, reactive residual Gd atoms are pushed towards solid/liquid interface and promote the nucleation for new grains. In addition, the volume fraction of the second phase increases with the increase of Gd content, which impedes the further growth of grains [17].

At the end of solidification, the alloy will bear thermal contraction resulted from solidification shrinkage. The fine grain structure cannot only easily accommodate the deformation resulted from thermal contraction due to a great number of grain boundaries, but also efficiently delay the onset of interdendritic feeding strength development. The delayed interdendritic feeding can shorten the practical susceptible temperature range of hot tearing. Furthermore, the number of paths for the liquid to flow increases due to the fine grain size, which can increase the refilling capacity and possibly heal the tears that formed previously. In contrast, Mg-6Zn-2Gd alloy has poor coordinating deformation capability due to the columnar grains with a large size. The columnar grains usually subject to a tensile stress perpendicular to the growth direction [26]. All of this can promote initiation and propagation of hot-tearing and lead to largest HTS value. To quantitatively explore the effect of grain size on HTS, Fig. 9(b) gives the variation of HTS with grain size. The mathematical relationship between HTS value and grain size (d) by a linear regression analysis can be expressed as follows:

$$HTS=14.56+0.037d \quad (5)$$

It can be seen that HTS decreases monotonously with decrease of the grain size. Therefore, it can be concluded that the fine equiaxed grains can reduce the HTS of Mg-6Zn-xGd alloys.

Figure 10 shows the hot tearing fracture surface of Mg-6Zn-xGd casting alloys. It is obvious that the content of eutectic

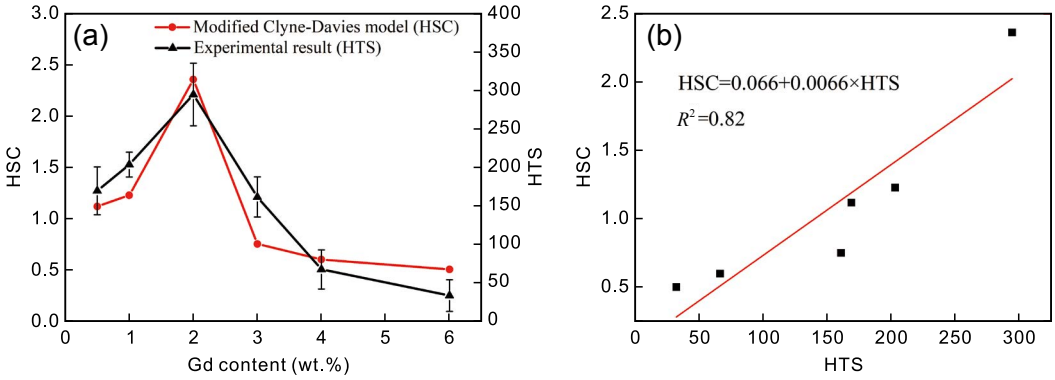

Fig. 7: HTS and HSC curves of Mg-6Zn-xGd(x=0.5, 1, 2, 3, 4, 6) casting alloys (a) and variation of HSC with HTS (b)

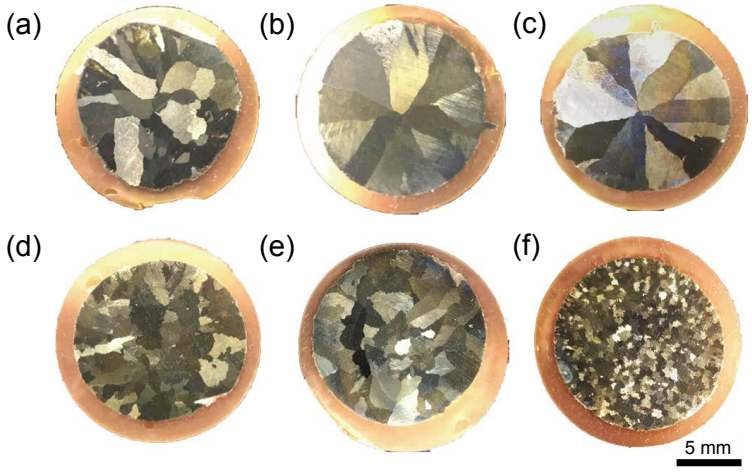

Fig. 8: OM images of Mg-6Zn-0.5Gd (a), Mg-6Zn-1Gd (b), Mg-6Zn-2Gd (c), Mg-6Zn-3Gd (d), Mg-6Zn-4Gd (e) and Mg-6Zn-6Gd (f) casting alloys

structure has no significant change when the Gd content is lower than 2%. With the further increase of Gd content, the eutectic phase volume increases gradually and then reaches the maximum for Mg-6Zn-6Gd alloy. According to the enlarged image marked by red dotted rectangle in Fig. 10(b), broken dendrite bridge is observed in Mg-6Zn-1Gd alloy. According to dendrite bridging theory, dendrite bridge can resist the crack propagation at the end of solidification process and increase the hot-tearing resistance of alloy. Though the dendrite bridge is broken, it indicates Mg-6Zn-1Gd alloy has relatively good hot-tearing resistance. In Mg-6Zn-3Gd and Mg-6Zn-4Gd alloys [Fig. 10(e) and Fig. 10(g)], dendrite-like bumps on the fracture surface and inter granular fracture are discerned, indicating that the formation of hot-tearing is caused by an interdendritic separation in the mushy zone. The ruptured liquid film on the dendrite can increase hot-tearing resistance to a certain extent. In addition, the complete dendrite bridge [Fig. 10(f)] further confirms the increase of hot-tearing resistance. In Mg-6Zn-4Gd alloy and Mg-6Zn-6Gd alloy [Fig. 10(g) and Fig. 10(i)], a higher volume fraction of continuous eutectic phase [Fig. 10(h)] forms due

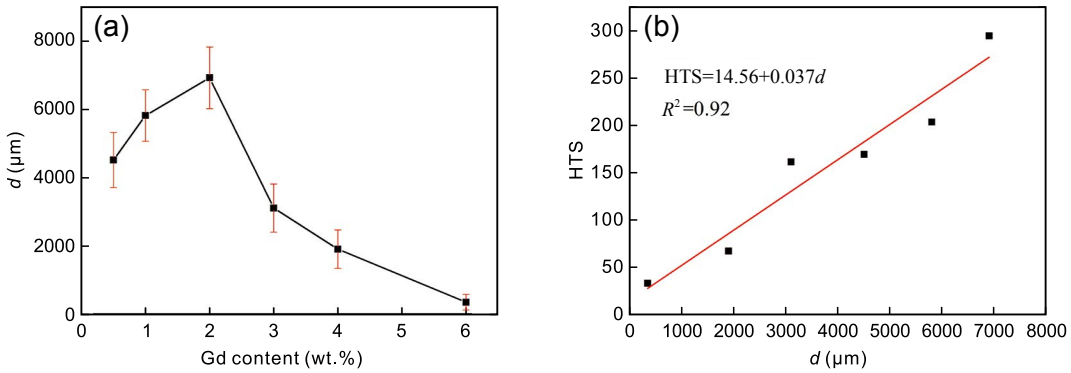

Fig. 9: Variation of grain size with Gd content (a) and HTS as a function of grain size (b)

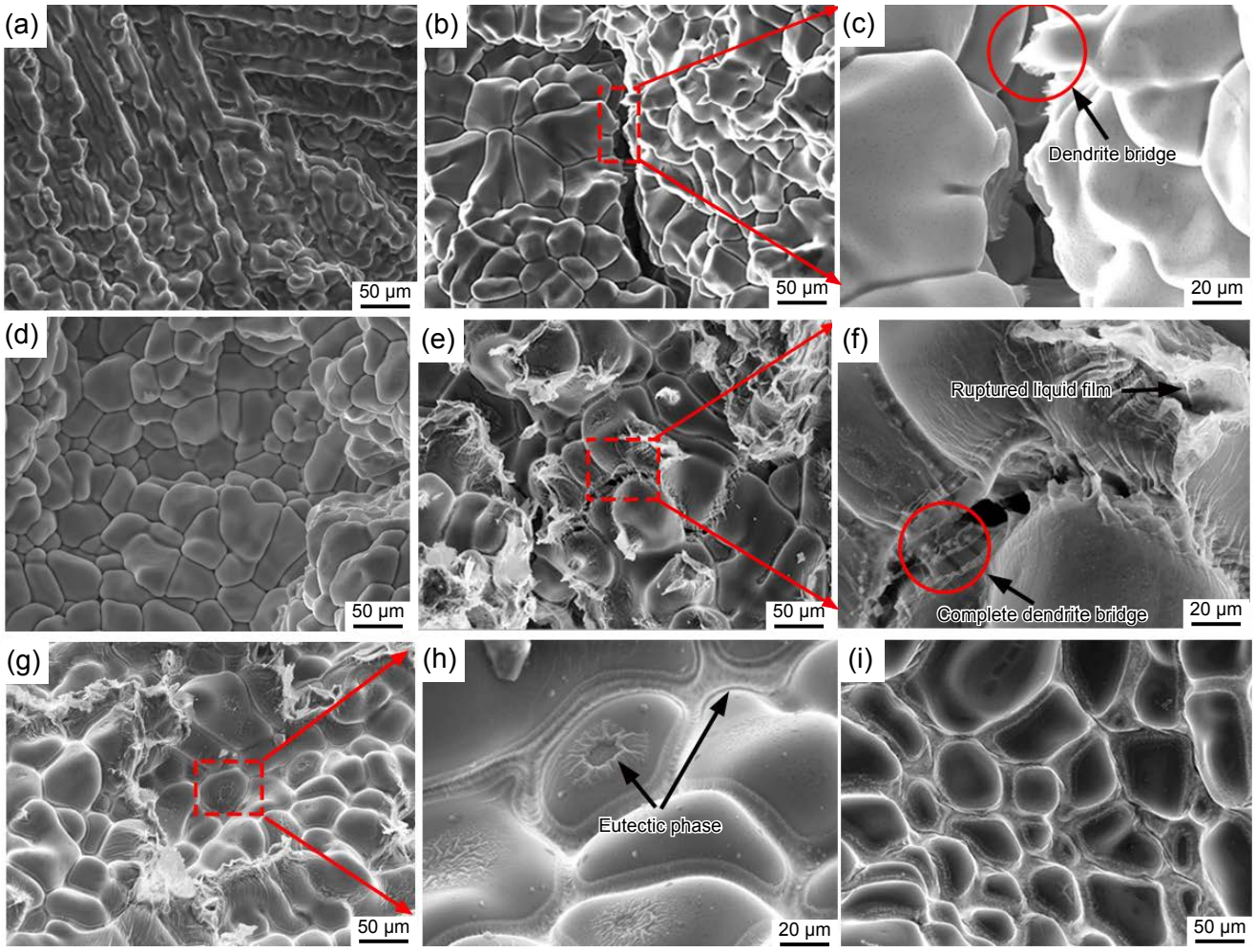

Fig. 10: Hot tearing fracture morphologies of Mg-6Zn-0.5Gd (a), Mg-6Zn-1Gd (b) and (c), Mg-6Zn-2Gd (d), Mg-6Zn-3Gd (e) and (f), Mg-6Zn-4Gd (g) and (h), and Mg-6Zn-6Gd alloys (i)

to a higher amount of the eutectic liquid at the final stage of solidification. Such a phenomenon strongly indicates that the presence of the abundant liquid is sufficient to refill the cracking when the tears occur. Comparing with Mg-6Zn-4Gd alloy, Mg-6Zn-6Gd alloy has the best hot-tearing resistance due to thicker liquid film.

Figure 11 shows the microstructures observed in the longitudinal sections of the rod near the hot sprue in the same position. It can be seen that Mg-6Zn-6Gd has the largest volume of eutectic liquid. As can be seen from Figs. 11(a) to (d), the volume of eutectic liquid is too low to refill the space between dendrite, which will lead to a higher hot tearing susceptibility at the final stage of solidification. According to the liquid film strain theory, a thin layer of liquid film surrounding the solid dendrites can lead to a strain concentration and cause the initiation of a tearing [27]. Figures 11(e) and (f) show SEM image of Mg-6Zn-4Gd and Mg-6Zn-6Gd, respectively. The eutectic phase totally fills the clearance between dendrite and the continuous feeding channels formed. The image with a higher magnification [Fig. 11(g)] of the eutectic phase clearly shows that the continuous net-shaped eutectic phase is consisted of α-Mg and W-phase as confirmed by EDS analysis in Fig. 11(h). As a result, Mg-6Zn-6Gd alloy has a better hot-tearing resistance due to the presence of W-phase (with a low melting point) and continuous feeding channels.

4 Conclusions

The HTS and hot-tearing behavior characteristics of Mg-6Zn-*x*Gd ternary casting alloys were investigated using a CRC mold and a multifunctional hot-tearing test device. Combining the grain size observation with fracture structure analysis, the hot tearing formation mechanism was further discussed. The following conclusions can be drawn:

(1) The HTS curve of Mg-6Zn-*x*Gd alloys as a function of Gd content follows the typical "Λ" shape: HTS increases firstly and then decreases with the increase of Gd content, and Mg-6Zn-2Gd alloy and Mg-6Zn-6Gd alloy have the highest and the lowest HTS values, respectively.

(2) The modified Clyne-Davies criterion according to the dendrite contact point can predict the hot tearing susceptibility well.

(3) The grain morphologies of Mg-6Zn-*x*Gd casting alloys change from mixed grain to columnar grain, mixed grain, and

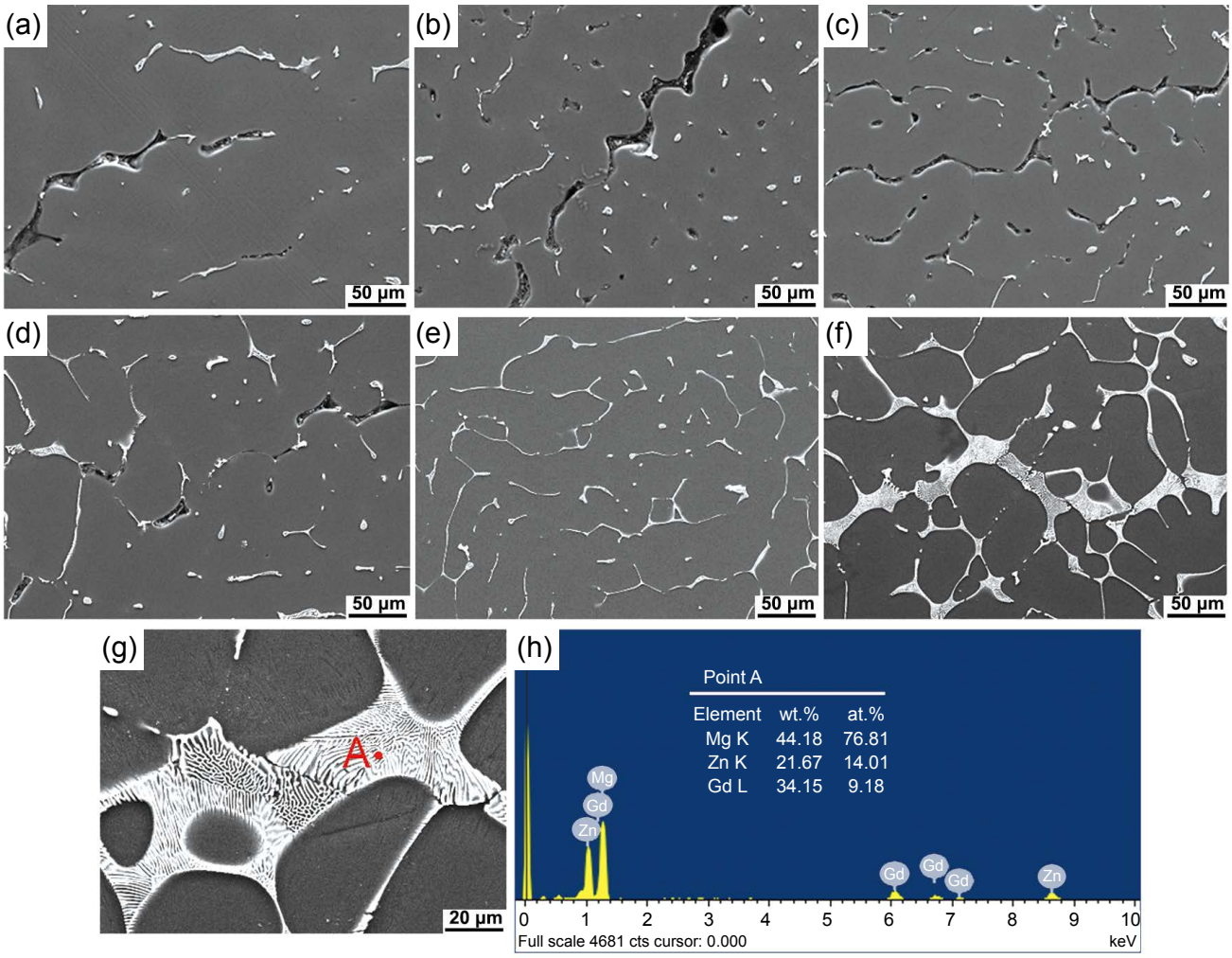

Fig. 11: SEM images of longitudinal sections for Mg-6Zn-0.5Gd (a), Mg-6Zn-1Gd (b), Mg-6Zn-2Gd (c), Mg-6Zn-3Gd (d), Mg-6Zn-4Gd (e), Mg-6Zn-6Gd (f) and (g) alloy, and EDS result of Point A in (g) (h)

equiaxed grain with the increase of Gd content. The larger grain size leads to the higher HTS due to the poor feeding and coordinating deformation capability.

(4) A higher volume fraction of eutectic phase can refill the cracking and provide continuous feeding channels by dendrite bridge and thicker liquid film, which increases hot-tearing resistance of Mg-6Zn-*x*Gd casting alloys.

Acknowledgements

This work was supported by the National Key R&D Program of China (Grant No. 2018YFB1106800), and the National Natural Science Foundation of China (Grant No. 51771152).

References

[1] Pan F S, Yang M B, Chen X H. A review on casting magnesium alloys: Modification of commercial alloys and development of new alloys. J. Mater. Sci. Technol., 2016, 32(12): 1211–1221.
[2] Song J F, She J, Chen D L, et al. Latest research advances on magnesium and magnesium alloys worldwide. J. Magnes. Alloy., 2020, 8(1): 1–41.
[3] Fu P H, Peng L M, Jiang H Y. Tensile properties of high strength cast Mg alloys at room temperature: A review. China Foundry, 2014, 11(4): 277–286.
[4] Xiao L, Yang G Y, Chen J M, et al. Microstructure, texture evolution and tensile properties of extruded Mg-4.58Zn-2.6Gd-0.16Zr alloy. Mater. Sci. Eng. A, 2019, 744: 277–289.
[5] Gao X, Nie J F. Characterization of strengthening precipitate phases in a Mg-Zn alloy. Scr. Mater., 2007, 56(8): 645–648.
[6] Zhang G J, Wang Y, Liu Z, et al. Influence of Al addition on solidification path and hot tearing susceptibility of Mg-2Zn-(3+0.5*x*)Y-*x*Al alloys. J. Magnes. Alloy., 2019, 7(2): 272–282.
[7] Zhou L, Huang Y D, Mao P L, et al. Influence of composition on hot tearing in binary Mg-Zn alloys. Int. J. Cast. Metal. Res., 2011, 24(3–4): 170–176.
[8] Clyne T W, Davies G J. The influence of composition on solidification cracking susceptibility in binary alloys. Br. Foundaryman, 1981, 74: 65–73.
[9] Zhou L, Huang Y D, Mao P L, et al. Investigation on hot tearing of Mg-Zn-(Al) alloys. Magnesium Technology, 2011: 125–130.
[10] Wang Z, Song J F D, Huang Y, et al. An investigation on hot tearing of Mg-4.5Zn-(0.5Zr) alloys with Y additions. Metall. Mater. Trans. A, 2015, 46(5): 2108–2118.
[11] Gunde P, Schiffl A, Uggowitzer P J. Influence of yttrium additions on the hot tearing susceptibility of magnesium-zinc alloys. Mater. Sci. Eng. A, 2010, 527(26): 7074–7079.
[12] Gao L, Chen R S, Han E H. Effects of rare-earth elements Gd and Y on the solid solution strengthening of Mg alloys. J. Alloys Compd., 2009, 481(1–2): 379–384.
[13] Zhan L, Le Y Z, Feng Z J, et al. Effect of Gd addition on mechanical and microstructural properties of Mg-*x*Gd-2.6Nd-0.5Zn-0.5Zr cast alloys. China Foundry, 2020, 17(3): 212–218.
[14] Yin S Q, Zhang Z Q, Liu X, et al. Effects of Zn/Gd ratio on the microstructures and mechanical properties of Mg-Zn-Gd-Zr alloys. Mater. Sci. Eng. A, 2017, 695: 135–143.
[15] Liu S J, Yang G Y, Luo S F, et al. Microstructure and mechanical properties of sand mold cast Mg-4.58Zn-2.6Gd-0.18Zr magnesium alloy after different heat treatments. J. Alloys Compd., 2015, 644: 846–853.
[16] Srinivasan A, Wang Z, Huang Y D, et al. Hot tearing characteristics of binary Mg-Gd alloy castings. Metall. Mater. Trans. A, 2013, 44A(5): 2285–2298.
[17] Luo S F, Yang G Y, Zou Z, et al. Hot tearing susceptibility of binary Mg-Gd alloy castings and influence of grain refinement. Adv. Eng. Mater., 2018, 20(8): 1800139.
[18] Cao G, Kou S. Hot cracking of binary Mg-Al alloy castings. Mater. Sci. Eng. A, 2006, 417(1–2): 230–238.
[19] Li J L, Chen R S, Ma Y Q, et al. Hot tearing of sand cast Mg-5wt.% Y-4wt.% RE (WE54) alloy. Acta Metall. Sin-Engl., 2013, 26(6): 728–734.
[20] Emadi D, Whiting L V, Nafisi S, et al. Applications of thermal analysis in quality control of solidification processes. J. Therm. Anal. Calorim., 2005, 81(1): 235–241.
[21] Huang Z H, Liang S M, Chen R S, et al. Solidification pathways and constituent phases of Mg-Zn-Y-Zr alloys. J. Alloys Compd., 2009, 468(1–2): 170–178.
[22] Suyitno, Kool W H, Katgerman L. Integrated approach for prediction of hot tearing. Metall. Mater. Trans. A, 2009, 40(10): 2388–2400.
[23] Shankar S, Riddle Y W, Makhlouf M M. Nucleation mechanism of the eutectic phases in aluminum-silicon hypoeutectic alloys. Acta Mater., 2004, 52(15): 4447–4460.
[24] Huang H, Fu P H, Wang Y X, et al. Effect of pouring and mold temperatures on hot tearing susceptibility of AZ91D and Mg-3Nd-0.2Zn-Zr Mg alloys. Trans. Nonferrous Met. Soc. China, 2014, 24(4): 922–929.
[25] Caceres C H, Blake A. The strength of concentrated Mg-Zn solid solutions. Phys. Stat. Sol. A, 2002, 194(1): 147–158.
[26] Easton M A, Wang H, Grandfield J, et al. Observation and prediction of the hot tear susceptibility of ternary Al-Si-Mg alloys. Metall. Mater. Trans. A, 2012, 43(9): 3227–3238.